Available online at www.sciencedirect.com
SCIENCE DIRECT®
Journal of Photochemistry and Photobiology A: Chemistry 157 (2003) 283–293
Journal of Photochemistry and Photobiology A:Chemistry
www.elsevier.com/locate/jphotochem

A visible and FTIR spectrometric study of the nighttime chemistry of acetaldehyde and PAN under simulated atmospheric conditions

J.F. Doussin*, B. Picquet-Varrault, R. Durand-Jolibois, H. Loirat, P. Carlier

Laboratoire Interuniversitaire des Systèmes Atmosphériques, UMR-CNRS 7583, Universités Paris 7 et Paris 12, 61 Avenue du Général De Gaulle, 94010 Créteil Cedex, France

Received 7 June 2002; received in revised form 10 December 2002; accepted 23 December 2002

Abstract

An atmospheric simulation chamber equipped with both a long path UV-visible spectrometer and an in situ Fourier transform infrared (FTIR) analysis device has been used to study the complete scheme of the nitrate radical initiated oxidation of acetaldehyde. This study constitutes one of the first evidence under simulated atmospheric conditions of the existence of reaction: $NO_3 + CH_3C(O)O_2 \rightarrow CH_3C(O)O + NO_2 + O_2$ which has been pointed out as an atmospherically important process in the nighttime OH production. Its rate constant at 298 ± 2 K has been found equal to $k = (3.2 \pm 1.4) \times 10^{-12}$ molecule^{-1} cm^3 s^{-1}.

Rate constants for the following reactions have also been determined at 298 ± 2 K; $HCHO + NO_3 \rightarrow HNO_3 + HCO$ with $k = (5.2 \pm 0.9) \times 10^{-16}$ molecule^{-1} cm^3 s^{-1} and $CH_3CHO + NO_3 \rightarrow HNO_3 + CH_3CO$ with $k = (2.1 \pm 0.7) \times 10^{-15}$ molecule^{-1} cm^3 s^{-1}.

Keywords: Acetaldehyde; Peroxyacetyl nitrate; FTIR; Nighttime chemistry; Nitrate radical; Atmospheric chemistry

1. Introduction

Aldehydes are emitted in the atmosphere as primary pollutants from the combustion of fossil fuels and are products of most of the atmospheric oxidation processes of volatile organic compounds. During the daytime, the major sinks of aldehydes are the photolysis and the reaction with OH radical. Aldehydes are continuously produced and at night, they react with the nitrate radical.

NO_3 is generated by the ozone oxidation of NO_2 (reaction 1). Nitrate radicals can be temporarily stored as dinitrogen pentoxide via the equilibrium (reactions 2,−2).

$$NO_2 + O_3 \rightarrow NO_3 + O_2 \quad (1)$$

$$NO_2 + NO_3 + M \rightleftharpoons N_2O_5 + M \quad (2,-2)$$

The NO_3-induced oxidation of aldehydes must be considered as a minor loss process in the atmosphere. However, the need of further work on the NO_3/aldehyde systems have been pointed out [1] in order to get a better understanding of this chemistry.

It is now obvious that nitrate radical reacts preferentially with aliphatic aldehydes through an overall aldehydic hydrogen abstraction. D'Anna and Nielsen [2] have investigated the kinetics of the oxidation of larger aldehydes by NO_3. Recently, Papagni et al. [3], Ullerstam et al. [4] and D'Anna et al. [5] have studied the kinetic of NO_3 with series of C3 to C6 aldehydes. They reported systematic deviations from the correlation between abstraction reactions with OH and with NO_3 proposed by Wayne et al. [1]. Additionally, Cabanas et al. [6] studied the temperature dependence for the gas-phase reactions of NO_3 a series of aliphatic aldehydes from C2 to C7. These authors suggested that the NO_3-initiated oxidation of aldehydes proceed via an adduct formation followed by C–H_{ald} bond cleavage.

The kinetic of the NO_3 reaction with acetaldehyde and formaldehyde have been presented in several papers [6–12].

$$HCHO + NO_3 \rightarrow HNO_3 + HCO \quad (3)$$

$$CH_3CHO + NO_3 \rightarrow HNO_3 + CH_3CO \quad (4)$$

Most of these studies were "relative rate" experiments and some disagreements remain, especially, when the rate constant was determined relatively to the equilibrium constant $K_{2,-2}$. Recent values published for k_4 and correction of older measurements from new reference values lead to an overall disagreement of 30%. This disagreement may be due to the $K_{2,-2}$ value used [7,9,13] or the rate constant for the reference VOC involved [12]. Furthermore, one may observe significantly higher values when low pressure absolute experiments have been performed [6,11,12].

* Corresponding author.

1010-6030/03/$ – see front matter © 2003 Elsevier Science B.V. All rights reserved.
doi:10.1016/S1010-6030(03)00060-1

The nighttime oxidation of acetaldehyde under conditions that lead to high NO_3 level, leads to the production of peroxyacetyl nitrate (PAN) [8] through the reaction of CH_3CO radicals with oxygen followed by subsequent NO_2 addition.

Peroxyacyls nitrate are products of great atmospheric concern because of their phytotoxic properties [14], their biological activities and the role they play in atmospheric chemistry as reservoir for nitrogen oxides. Similarly to nitrate radicals, peroxyacyl radicals are involved in an equilibrium with NO_2 leading respectively to PANs and to N_2O_5 (reaction 5,−5 for PAN)

$$NO_2 + CH_3C(O)O_2 + M \rightleftharpoons CH_3C(O)O_2NO_2 + M \quad (5,-5)$$

To date, only one research group has investigated the nighttime chemistry of PAN [15]. They have shown that one of the key reaction was the reduction of the peroxyacetyl (PA) to acetyl radicals by NO_3 (reaction 6).

$$NO_3 + CH_3C(O)O_2 \rightarrow CH_3C(O)O + NO_2 + O_2 \quad (6)$$

The reported [16] rate constant for reaction (6) was $k_6 = (4 \pm 1) \times 10^{-12}\,cm^3\,molecule^{-1}\,s^{-1}$. This value was obtained from experiments conducted in a flow reactor connected to a fluorescence cell. The temperatures, pressures and concentration ranges were very different from the atmospheric conditions. Canosa-Mas et al. [16] have shown, by computer simulations and calculations from field studies results, that one of the atmospheric implications of this reaction could be a significant production of OH radicals at night. Recently, D'Anna et al. [12] had to reduced the k_6 value by more than an order of magnitude to reproduce by computer simulation their experimental results. This disagreement between the two only work involving the determination of k_6, led us to investigate this reaction.

The present paper report simulation chamber investigations of the complete scheme of the atmospheric degradation of acetaldehyde at room temperature and atmospheric pressure. Kinetics and mechanistic information about reactions 3, 4 and 6 are derived from the computer simulation of obtained experimental data.

2. Experimental

2.1. Simulation chamber

The experimental device used in the present study has been previously presented in detail [17] and only a brief description need to be given here. Experiments were performed in a large Pyrex® reactor (6 m length, 0.45 m diameter and 977 l volume). A multiple reflection White type mirror system was included in the chamber to give a total path length of 72 m in the UV-visible range. The UV-visible spectrometer was made of a 450 W XBO source and of Czerny-turner Jobin-Yvon™ monochromator connected to a photomultiplicator. The slit width was adjusted to give a resolution equal to 0.5 nm.

In parallel with the UV-visible, Fourier transform infrared (FTIR) spectrometry was used. A stabilized multiple reflection cell [18] derived from the White type arrangement was set up to offer a total path length of 96 m. This mirror arrangement was coupled to a Bomem™ DA-8 spectrometer. Spectra were obtained by co-adding 30–60 scans recorded at $0.7\,cm^{-1}$ apodized resolution. The scanning mirror speed was adjusted to allow us to record spectra every 30 s.

2.2. Chemicals

Experiments were performed in synthetic air (78% N_2 >99.95%, Air Liquide + 22% O_2 >99.95%, Air Liquide) at 298 ± 2 K and 1013 ± 10 mbar. Acetaldehyde (99.5%, Aldrich) purity was checked by GC-FID and by FTIR spectroscopy. Nitrate radical was generated from the thermal dissociation of N_2O_5. Dinitrogen pentoxide was prepared in a special slow flow reactor directly connected to the chamber by mixing during few seconds a known quantity of NO (>99.9%, Air Liquide) and a 5‰ O_3/O_2 mixture in an appropriate flow rate. Ozone was produced from oxygen (O_2, N45 Air Liquide) in a silent discharge generator (OZ 1000-L, Kauffmann Umwelttechnik).

2.3. Spectrometric analysis

Nitrate radical concentrations were monitored by absolute monochannel visible spectrometry using its absorption at 662 nm (Fig. 1). A synthetic reference spectrum was built in the 662 nm region from the high resolution experimental points from Sander [19], the band shape from Marinelli et al. [20] and the absorption cross-section proposed by Wayne et al. [1].

Light intensity transmitted through the chamber at 662 nm was continuously measured. The reference level was extrapolated from the period before the $N_2O_5/O_2/O_3$ mixture injection.

Time dependant concentrations of CH_3CHO, HCHO, PAN, N_2O_5, HNO_3, O_3, CO and CO_2 were monitored from their infrared spectral absorption. Infrared spectra of

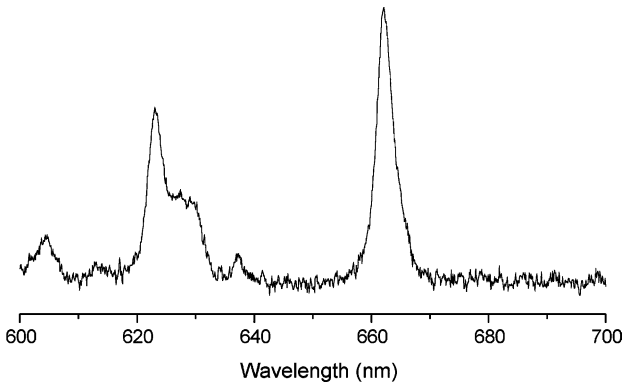

Fig. 1. Nitrate radical spectrum in the visible region (this work).

Table 1
Integrated band intensities from the reference spectra used in this study

Compounds	Wavenumbers (cm^{-1})	IBI, base e ($cm\ molecule^{-1}$)	Reference
N_2O_5	1205–1275	$(4.0 \pm 0.1) \times 10^{-17}$	[34,35]
HNO_3	840–930	$(2.2 \pm 0.2) \times 10^{-17}$	[36]
O_3	2015–2140	$(1.39 \pm 0.07) \times 10^{-18}$	[37]
CH_3CHO	1679–1828	$(2.0 \pm 0.2) \times 10^{-17}$	This work
HCHO	3000–2630	$(3.0 \pm 0.1) \times 10^{-17}$	[38]
PAN	1100–1190	$(1.90 \pm 0.04) \times 10^{-17}$	[39]
CO_2	2280–2400	$(9.57 \pm 0.04) \times 10^{-17}$	[37]
CO	2030–2250	$(9.69 \pm 0.04) \times 10^{-18}$	[37]

Errors given are random and expressed as 95% confidence limits or otherwise stated in the cited article.

aldehydes were calibrated by introducing small quantities of HCHO and CH_3CHO into the chamber and sampling in DNPH solution for HPLC analysis. Other calibration were taken from literature. Integrated band intensities (IBI) of the main absorption bands of these compounds are given in Table 1.

2.4. Experimental procedure

The nighttime chemistry of acetaldehyde and PAN was studied by performing five different experiments in the simulation chamber. The initial concentrations used during these experiments are summarised in Table 2.

Each experiment was divided within two periods: first, nitrate radical was generated in synthetic air ("blank experiment"), then when the NO_3 concentration were close to zero a second injection of the nitrate generation mixture were performed in presence of the studied VOC.

This procedure allowed us to determine the parameters that depend on experimental conditions such as the extent of the N_2O_5 heterogeneous reaction or the NO_3 photolysis induced by the UV-visible analysis light beam.

Furthermore, the design used to produce N_2O_5/NO_3 led us to work with relatively high ozone concentration (10–100 ppm). This characteristic of our experiments was chosen on purpose to allow us to evaluate the OH/HO_2 concentrations arising from the VOC chemistry (see below).

Experiments were numerically simulated using Facsimile® software package [21].

3. Results

During the experiments, nine compounds (e.g. CO, CO_2, HCHO, PAN, CH_3CHO, HNO_3, N_2O_5, NO_3 and O_3) were detected and monitored.

3.1. Temporal behaviors of reactants and products

3.1.1. Nitrate radical

Fig. 2 shows the concentration-time profiles of monitored compounds during NO_3 induced oxidation of acetaldehyde. Without VOC, the behavior of NO_3 in the chamber is mainly driven by the N_2O_5 heterogeneous reaction

$$N_2O_5 + \text{adsorbed water on wall} \rightarrow HNO_3 \quad (7)$$

One can observe that the apparent nitrate radical lifetime is considerably reduced in presence of acetaldehyde. This can be easily explained by the reactions with acetaldehyde and its oxidation intermediates (reactions 3, 4, 6 or 13), which lead to stable products such as HNO_3. These processes constitute additional sinks for NO_3 and, hence, induce a reduction of the N_2O_5 lifetime.

Reactions between nitrate radicals and peroxy radicals such as reaction 6 must also be taken into account as a sink for NO_3 leading to NO_2. It can be shown from the ozone and NO_3 profiles and from the rate constants for reactions 1 and 2 that the major fate of NO_2 in the reactant mixture is reaction 2 as long as NO_3 concentration is higher than 6×10^{10} molecule cm^{-3}. Hence, the production of NO_2 can be considered as a partial sink of NO_3 as most of N_2O_5 is converted into nitric acid by reaction 7.

After a fast decrease, the NO_3 concentration seems to exhibit oscillations. This phenomenon is close to our detection limit and could be the sign of residual quantities of NO_3. Nitrate radical concentration would then be maintained to a non-zero value by the NO_x regeneration from the slow decomposition of PAN (reaction −5).

3.1.2. Acetaldehyde

The main pattern in the concentration-time behaviour of acetaldehyde is a consumption divided into two phases. At the $N_2O_5/O_2/O_3$ mixture injection, one can observe a very fast decrease of the CH_3CHO concentration due to reaction 4. Then, when the concentration of NO_3 is very low, the

Table 2
Initial condition used for the room temperature experiments: (1) at the beginning of the acetaldehyde oxidation; (2) during blank experiments i.e. without acetaldehyde; (3) when acetaldehyde present

Experiment	$[CH_3CHO]_0$, ppm	$[O_3]_0$ (1), ppm	$[NO_3]_{max}$, (2) ppb	$[NO_3]_{max}$, (3) ppb	Remark
CH_3CHO#1	7.2	120	320	100	
CH_3CHO#2	7.2	16	190	44	
CH_3CHO#3	6.1	101	192	39	Three NO_3 radical generation experiment
CH_3CHO#4	6.2	86	134	42	Three NO_3 radical generation experiment
CH_3CHO#5	7.2	93	169	37	Three NO_3 radical generation experiment

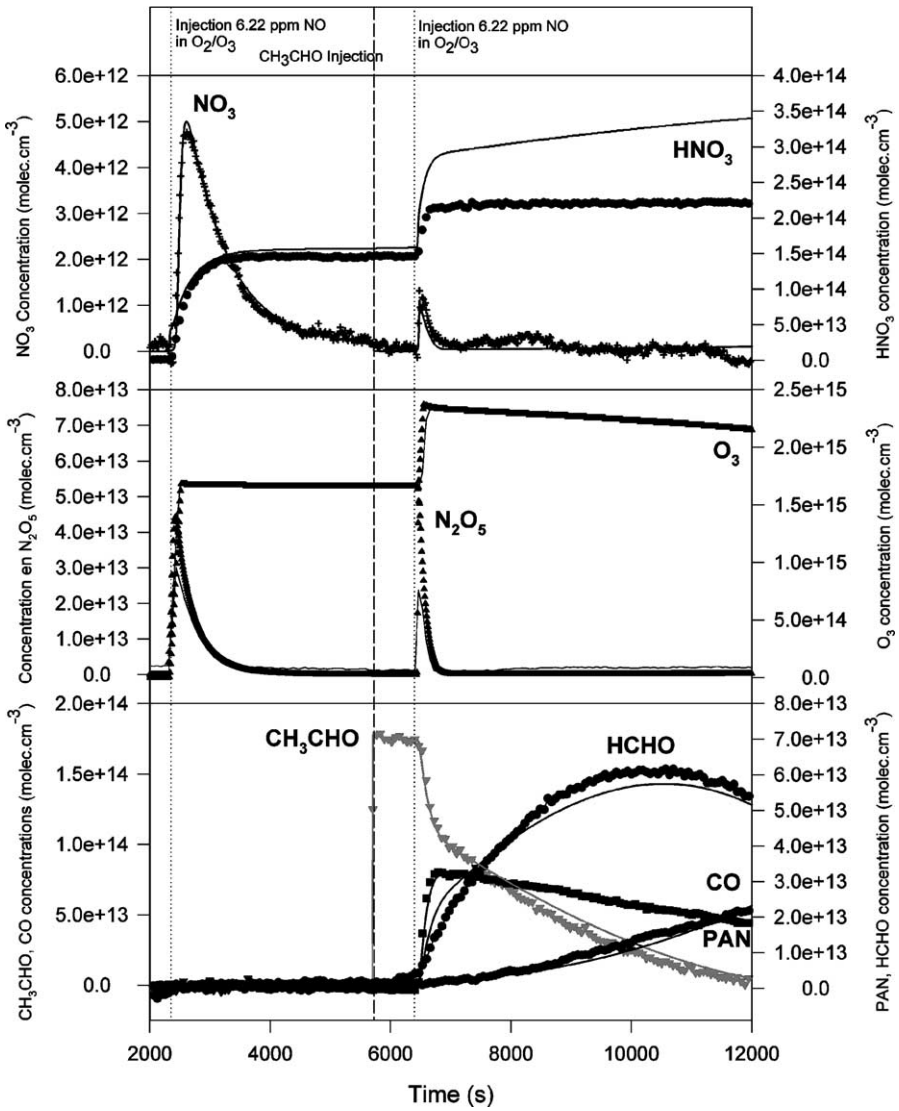

Fig. 2. Temporal profile of measured compounds during an experiment of NO_3 induced oxidation of acetaldehyde (dots are experimental data, lines are simulated concentrations).

acetaldehyde decrease remains fairly fast. Such a decreasing rate cannot be explained solely by residual NO_3. This seems to indicate that an OH radical dark production must be taken into account. A hypothetical oxidation scheme, which shows an OH production pathway, is given in Fig. 3. The change in the slope of the acetaldehyde profile defines the change from the "NO_3 driven chemistry" to the "OH driven chemistry".

3.1.3. Organic products

In the studied system, PAN is formed by the following reaction sequence:

$$CH_3CHO + NO_3 \rightarrow HNO_3 + CH_3CO \quad (4)$$

$$CH_3CO + O_2 + M \rightarrow CH_3C(O)O_2 + M \quad (8)$$

$$NO_2 + CH_3C(O)O_2 + M \rightarrow CH_3C(O)O_2NO_2 + M \quad (5)$$

Its profile shows a fast increase in the first period of the reaction with an apparent formation yield close to 70%. This can be easily explained by the fact that this period is characterized by the highest acetaldehyde and NO_3 concentrations and consequently the highest peroxyacetyl radicals and NO_2 levels.

At the limit between the "NO_3 driven chemistry" and the "OH driven chemistry" periods, PAN concentrations reach their maximum. Then, the peroxyacetyl consumption reactions (6, 9, 10) shift the PAN equilibrium (5,−5) leading to a slow decrease of PAN.

$$NO_3 + CH_3C(O)O_2 \rightarrow CH_3C(O)O + NO_2 + O_2 \quad (6)$$

$$2CH_3C(O)O_2 \rightarrow 2CH_3C(O)O + O_2 \quad (9)$$

$$CH_3C(O)O + O_2 \rightarrow CH_3 + CO_2 + O_2 \quad (10)$$

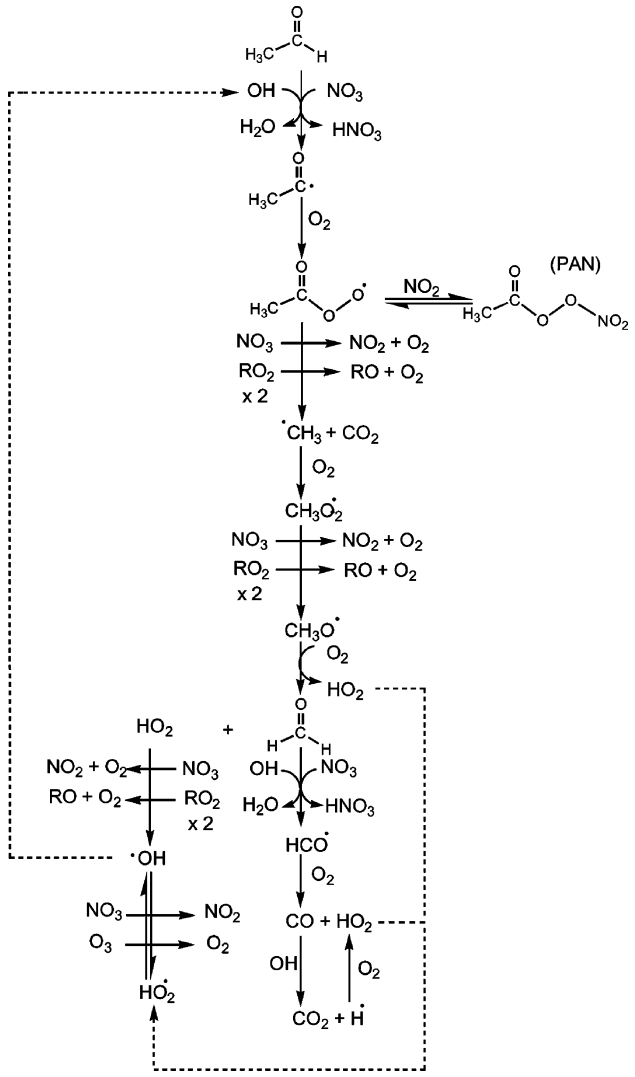

Fig. 3. Scheme of NO_3 induced oxidation of acetaldehyde under present experimental conditions.

Peroxyacetyl decomposition leads to the formation of methyl radicals that react further to give formaldehyde (11–14).

$$CH_3 + O_2 + M \rightarrow CH_3O_2 + M \quad (11)$$

$$2CH_3O_2 + M \rightarrow 2CH_3O + M \quad (12)$$

$$CH_3O_2 + NO_3 \rightarrow CH_3O + NO_2 + O_2 \quad (13)$$

$$CH_3O + O_2 \rightarrow HCHO + HO_2 \quad (14)$$

$$HO_2 + NO_3 \rightarrow OH + NO_2 + O_2 \quad (15)$$

Furthermore, this sequence constitutes the principal homogeneous pathway to form HO_2 in the chamber. This could explain why sufficient OH concentrations remain during the "OH driven chemistry" period to induce the observed acetaldehyde consumption.

Formaldehyde is detected as soon as acetaldehyde is injected. Its formation in the very beginning of the second

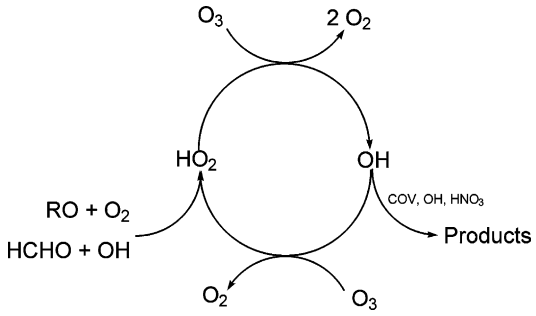

Fig. 4. Ozone consumption cycle.

phase of the experiments can be explained by a slow consumption of acetaldehyde by residual nitrate radicals. Then, at the $N_2O_5/O_2/O_3$ mixture injection the production rate of formaldehyde increases. Reaction 12 followed by reaction 14 is the main production pathway. It should be noted that HCHO is consumed all along the experiments by reaction 3. This reaction followed by reaction 16 constitute an additional OH production pathway.

$$HCO + O_2 + M \rightarrow HO_2 + CO + M \quad (16)$$

Relatively high quantities of ozone are injected with the nitrate radicals precursors mixture. These concentrations remain fairly stable during the blank experiments but when acetaldehyde is present a slow decrease of ozone is noticed. This behavior can be interpreted as the effect of the inter-conversion cycle between HO_2 and OH (Fig. 4)

3.2. Multiple nitrate radical generations experiments

In order to enhance the effect of nitrate radical on secondary product concentrations, a third $N_2O_5/O_2/O_3$ mixture was performed during three of the five experiments described here (see Table 2).

During the experiment shown in Fig. 5, the third NO_3 radicals in situ generation was performed when PANs concentrations were high and aldehydes concentrations were low. In the $N_2O_5/O_2/O_3$ mixture used the NO_x content was adjusted to generate more NO_3.

At the third NO_3 production, HCHO concentrations decrease rapidly, leading to the production of CO. The most important feature shown during these experiments is the fact that PAN concentrations decrease is visibly enhanced by the increase of the NO_3 concentrations. This observation constitutes the first direct evidence at atmospheric pressure and in the ppm range of the reaction between NO_3 and PA radicals. From the rate constant of the reaction between PAN and OH[23] it is possible to assume that the reaction between PAN and NO_3 is very slow. The additional PAN loss is then explained by the following sequence:

$$CH_3C(O)O_2NO_2 + M \rightleftharpoons NO_2 + CH_3C(O)O_2 + M \quad (-5,5)$$

$$NO_3 + CH_3C(O)O_2 \rightarrow CH_3C(O)O + NO_2 + O_2 \quad (6)$$

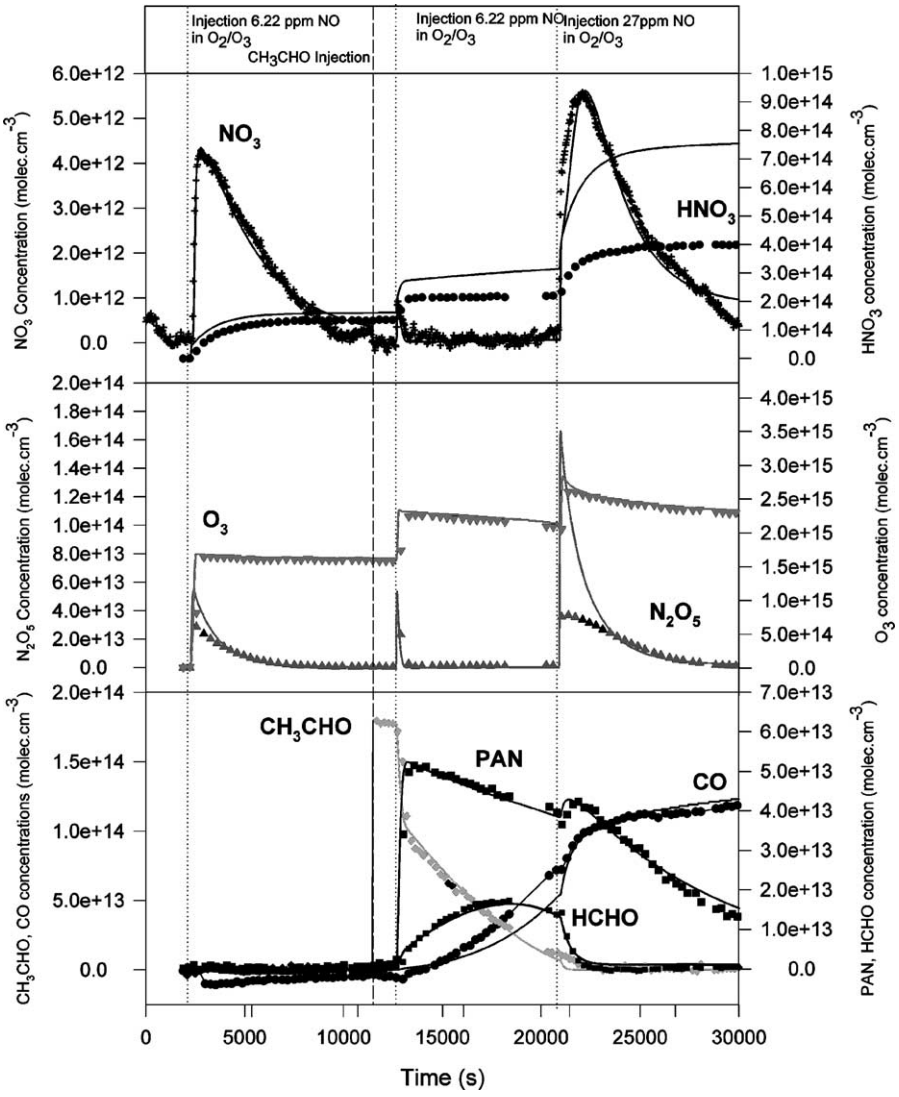

Fig. 5. Temporal profile of measured compounds during a three-stages experiment of NO_3 induced oxidation of acetaldehyde (dots are experimental data, lines are simulated concentrations).

4. Discussion

4.1. Computer simulation data analysis

The concentration-time profile obtained from both FTIR and UV-visible spectrometry were analyzed using the AEA computer program facsimile [21]. An explicit model including 63 reactions has been used and appropriate rates constant were selected from recent compiled table. Table 3 shows the reactions that describe the homogeneous gas-phase part of the proposed mechanism. The experimental conditions dependent rates and the poorly known rate constants were adjusted in order to fit experimental curves. The related reactions are indicated in bold on Table 3.

From Fig. 6, it can be seen that simulated results and experimental data are in reasonable agreement during the "NO_3 driven chemistry periods" but they show strong divergence when NO_3 concentration become low. One can see that acetaldehyde consumption and the product build up are calculated too slow during that phase. These observations seem to indicate that too few dark OH are produced. On the other hand, it can be seen that the slow ozone consumption is underestimated.

The average OH level has been evaluated from a simple first-order analysis of the acetaldehyde decrease at low NO_3 level. This approach led us to an OH concentration of 3×10^7 radical cm^{-3}.

Many additional hypothetical processes have been considered in order to explain this unexpected behavior. Among these hypotheses, we have investigated the effect of slow reactions between peroxy radicals and ozone and between peroxyacyl radicals and ozone. This modified chemical

Table 3

Number	Rate constant	Reaction	Reference
1	1.9×10^{-14} cm^3 molecule^{-1} s^{-1}	$NO + O_3 \rightarrow NO_2 + O_2$	[40]
	3.5×10^{-17} cm^3 molecule^{-1} s^{-1}	$NO_2 + O_3 \rightarrow NO_3 + O_2$	[41]
2	1.3×10^{-12} cm^3 molecule^{-1} s^{-1}	$NO_2 + NO_3$ (+M) $\rightarrow N_2O_5$ (+M)	[41]
	2.6×10^{-11} cm^3 molecule^{-1} s^{-1}	$NO_3 + NO \rightarrow 2NO_2$	[41]
	5.1×10^{-16} cm^3 molecule^{-1} s^{-1}	$NO_2 + NO_3 \rightarrow NO + O_2 + NO_2$	[30]
	2.3×10^{-16} cm^3 molecule^{-1} s^{-1}	$NO_3 + NO_3 \rightarrow 2NO_2 + O_2$	[30]
−2	4.5×10^{-2} s^{-1}	N_2O_5 (+M) $\rightarrow NO_2 + NO_3$ (+M)	[30]
	$1 \times 10^{-5} - 5 \times 10^{-4}$ s^{-1}	**$NO_3 \rightarrow NO + O_2$**	[30]
	$4 \times 10^{-4} - 7 \times 10^{-3}$ s^{-1}	**N_2O_5 (+H_2O) $\rightarrow$ 2HNO_3**	[30]
4 + 7	2.7×10^{-15} molecule^{-1} cm^{-3} s^{-1}	**$CH_3CHO + NO_3 \rightarrow CH_3CO_3 + HNO_3$**	[41]
5	8.7×10^{-12} molecule^{-1} cm^{-3} s^{-1}	$CH_3CO_3 + NO_2$ + (M) $\rightarrow$ PAN + (M)	[41]
−5	3.16×10^{-4} s^{-1}	PAN + (M) $\rightarrow CH_3CO_3 + NO_2$ + (M)	[41]
	2.0×10^{-11} molecule^{-1} cm^{-3} s^{-1}	$CH_3CO_3 + NO \rightarrow CH_3O_2 + NO_2 + CO_2$	[30]
6 + 10	4.0×10^{-12} molecule^{-1} cm^{-3} s^{-1}	**$CH_3CO_3 + NO_3 \rightarrow CH_3O_2 + NO_2 + O_2 + CO_2$**	[16]
9 + 10	1.5×10^{-11} molecule^{-1} cm^{-3} s^{-1}	$CH_3CO_3 + CH_3CO_3 \rightarrow CH_3O_2 + CH_3O_2 + CO_2 + CO_2 + O_2$	[41]
	1.1×10^{-11} molecule^{-1} cm^{-3} s^{-1}	$CH_3CO_3 + CH_3O_2 \rightarrow CH_3O + CH_3O_2 + CO_2 + O_2$	[41]
	1.8×10^{-12} molecule^{-1} cm^{-3} s^{-1}	$CH_3CO_3 + CH_3O_2 \rightarrow HCHO + CH_3C(O)OH + O_2$	[41]
	1.0×10^{-11} molecule^{-1} cm^{-3} s^{-1}	$CH_3CO_3 + HO_2 \rightarrow CH_3C(O)OOH + O_2$	[41]
	3.6×10^{-12} molecule^{-1} cm^{-3} s^{-1}	$CH_3CO_3 + HO_2 \rightarrow CH_3C(O)OH + O_3$	[41]
	5.7×10^{-17} molecule^{-1} cm^{-3} s^{-1}	$CH_3CO_3 + CH_3CHO \rightarrow CH_3C(O)OOH + CH_3CO_3$	[42]
	7.5×10^{-12} molecule^{-1} cm^{-3} s^{-1}	$CH_3O_2 + NO \rightarrow CH_3O + NO_2$	[41]
	4.2×10^{-12} molecule^{-1} cm^{-3} s^{-1}	$CH_3O_2 + NO_2 \rightarrow CH_3O_2NO_2$	[41]
	2.41 s^{-1}	$CH_3O_2NO_2 \rightarrow CH_3O_2 + NO_2$	[41]
13	1.2×10^{-12} molecule^{-1} cm^{-3} s^{-1}	$CH_3O_2 + NO_3 \rightarrow CH_3O + NO_2 + O_2$	[41]
	5.2×10^{-12} molecule^{-1} cm^{-3} s^{-1}	$CH_3O_2 + HO_2 \rightarrow CH_3OOH + O_2$	[41]
	5.5×10^{-12} molecule^{-1} cm^{-3} s^{-1}	$OH + CH_3OOH \rightarrow CH_3O_2 + H_2O$	[30]
	3.7×10^{-13} molecule^{-1} cm^{-3} s^{-1}	$CH_3O_2 + CH_3O_2 \rightarrow 0.48CH_3O + O_2 + 0.76CH_3OH + 0.76HCHO$	[30]
12	3.7×10^{-14} molecule^{-1} cm^{-3} s^{-1}	$CH_3O_2 + CH_3O_2 \rightarrow CH_3OOCH_3 + O_2$	[30]
14	1.9×10^{-15} molecule^{-1} cm^{-3} s^{-1}	$CH_3O + O_2 \rightarrow HCHO + HO_2$	[41]
	2.0×10^{-11} molecule^{-1} cm^{-3} s^{-1}	$CH_3O + NO_2 \rightarrow CH_3ONO_2$	[41]
	3.7×10^{-13} molecule^{-1} cm^{-3} s^{-1}	$CH_3O + NO_2 \rightarrow HCHO + HONO$	[30]
	1.0×10^{-15} molecule^{-1} cm^{-3} s^{-1}	$CH_3O + HCHO \rightarrow CH_3OH + HO_2 + CO$	[42]
	2.0×10^{-13} molecule^{-1} cm^{-3} s^{-1}	$CH_3O + CH_3CHO \rightarrow CH_3OH + CH_3CO_3$	[42]
3 + 16	5.8×10^{-16} molecule^{-1} cm^{-3} s^{-1}	**$HCHO + NO_3 \rightarrow HNO_3 + HO_2 + CO$**	[41]
	2.4×10^{-16} molecule^{-1} cm^{-3} s^{-1}	$CH_3OH + NO_3 \rightarrow 0.5CH_3O + HNO_3 + 0.5CH_2OH$	[30]
	9.4×10^{-12} molecule^{-1} cm^{-3} s^{-1}	$CH_2OH + O_2 \rightarrow HCHO + HO_2$	[30]
	1.1×10^{-13} molecule^{-1} cm^{-3} s^{-1}	$PAN + OH \rightarrow HCHO + H_2O + NO_2 + CO_2$	[30]
	1.6×10^{-11} molecule^{-1} cm^{-3} s^{-1}	$CH_3CHO + OH \rightarrow CH_3CO_3 + H_2O$	[30]
	1.0×10^{-11} molecule^{-1} cm^{-3} s^{-1}	$HCHO + OH \rightarrow H_2O + HO_2 + CO$	[41]
	9.3×10^{-13} molecule^{-1} cm^{-3} s^{-1}	$CH_3OH + OH \rightarrow 0.15CH_3O + H_2O + 0.85CH_2OH$	[30]
	3.5×10^{-13} molecule^{-1} cm^{-3} s^{-1}	$CH_3ONO_2 + OH \rightarrow CH_3O + HNO_3$	[30]
	2.1×10^{-13} molecule^{-1} cm^{-3} s^{-1}	$CO + OH \rightarrow HO_2 + CO_2$	[30]
	7.9×10^{-14} molecule^{-1} cm^{-3} s^{-1}	$HO_2 + HCHO \rightarrow HOCH_2OO$	[41]
	150 s^{-1}	$HOCH_2OO \rightarrow HO_2 + HCHO$	[41]
	1.2×10^{-11} molecule^{-1} cm^{-3} s^{-1}	$HO_2 + HOCH_2OO \rightarrow 0.5HCOOH + 0.5HOCH_2O_2H + O_2 + 0.5H_2O$	[30]
	1.0×10^{-15} molecule^{-1} cm^{-3} s^{-1}	$HO_2 + CH_3CHO \rightarrow HOC_2H_4OO$	[30]
	100 s^{-1}	$HOC_2H_4OO \rightarrow HO_2 + CH_3CHO$	[30]
	1.0×10^{-11} molecule^{-1} cm^{-3} s^{-1}	$HO_2 + HOC_2H_4OO \rightarrow 0.5CH_3COOH + 0.5HOC_2H_4O_2H + O_2 + 0.5H_2O$	[30]
	1.0×10^{-3} s^{-1}	$HOCH_2O_2H \rightarrow H_2O + HC(O)OH$	[42]
	1.0×10^{-3} s^{-1}	$HOC_2H_4O_2H \rightarrow H_2O + CH_3C(O)OH$	[42]
	2.0×10^{-11} molecule^{-1} cm^{-3} s^{-1}	$OH + NO_3 \rightarrow HO_2 + NO_2$	[41]
	7.8×10^{-14} molecule^{-1} cm^{-3} s^{-1}	$OH + O_3 \rightarrow HO_2 + O_2$	[40]
	1.1×10^{-10} molecule^{-1} cm^{-3} s^{-1}	$OH + HO_2 \rightarrow H_2O + O_2$	[40]
	1.5×10^{-13} molecule^{-1} cm^{-3} s^{-1}	$OH + HNO_3 \rightarrow H_2O + NO_3$	[30]
	1.0×10^{-11} molecule^{-1} cm^{-3} s^{-1}	$OH + NO_2 \rightarrow HNO_3$	[41]
	1.9×10^{-12} molecule^{-1} cm^{-3} s^{-1}	$OH + OH$ (+O_2) $\rightarrow H_2O + O_3$	[41]
	6.3×10^{-12} molecule^{-1} cm^{-3} s^{-1}	$OH + OH \rightarrow H_2O_2$	[30]
	8.4×10^{-12} molecule^{-1} cm^{-3} s^{-1}	$OH + NO \rightarrow HONO$	[30]
	6.5×10^{-12} molecule^{-1} cm^{-3} s^{-1}	$OH + HONO \rightarrow H_2O + NO_2$	[41]

Table 3 (*Continued*)

Number	Rate constant	Reaction	Reference
	1.39×10^{-12} molecule^{-1} cm^{-3} s^{-1}	$HO_2 + NO_2 \rightarrow HO_2NO_2$	[41]
	5.0×10^{-16} molecule^{-1} cm^{-3} s^{-1}	$HO_2 + NO_2 \rightarrow HONO + O_2$	[41]
	2.0×10^{-15} molecule^{-1} cm^{-3} s^{-1}	$HO_2 + O_3 \rightarrow OH + O_2 + O_2$	[40]
	2.9×10^{-12} molecule^{-1} cm^{-3} s^{-1}	$HO_2 + HO_2 \rightarrow H_2O_2 + O_2$	[41]
	8.5×10^{-12} molecule^{-1} cm^{-3} s^{-1}	$HO_2 + NO \rightarrow OH + NO_2 + O_2$	[41]
15	2.0×10^{-12} molecule^{-1} cm^{-3} s^{-1}	$\mathbf{HO_2 + NO_3 \rightarrow OH + NO_2 + O_2}$	[41]
	2.0×10^{-12} molecule^{-1} cm^{-3} s^{-1}	$\mathbf{HO_2 + NO_3 \rightarrow HNO_3 + O_2}$	[41]
	0.09 s^{-1}	$HO_2NO_2 \rightarrow HO_2 + NO_2$	[30]
	2.5×10^{-12} molecule^{-1} cm^{-3} s^{-1}	$HO_2NO_2 + OH \rightarrow H_2O + O_2 + NO_2$	[41]
	2.5×10^{-12} molecule^{-1} cm^{-3} s^{-1}	$HO_2NO_2 + OH \rightarrow H_2O_2 + NO_3$	[30]
	1.7×10^{-12} molecule^{-1} cm^{-3} s^{-1}	$H_2O_2 + OH \rightarrow H_2O + HO_2$	[41]

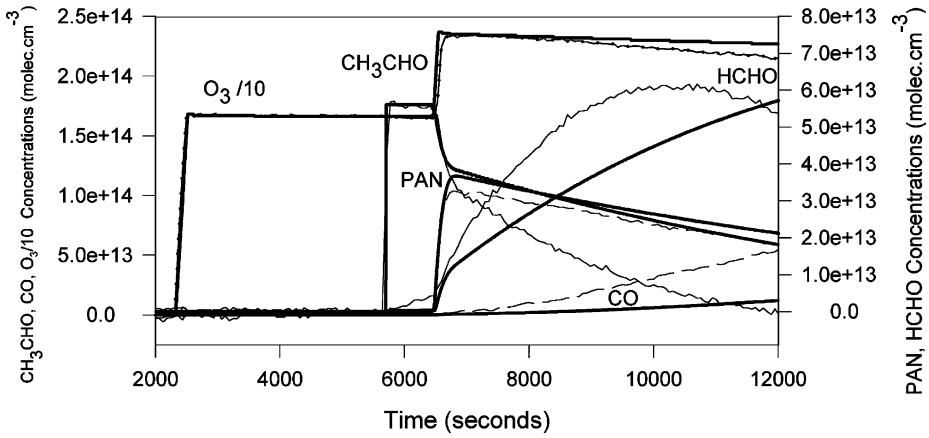

Fig. 6. Comparison between the temporal profile of measured concentrations (thin line) and simulated concentrations (bold line) using the model described in Table 3.

mechanism led us to a poor agreement between simulated and experimental concentrations and the adjusted values for the rate constants of these additional reactions were one order of magnitude higher than the upper limit reported by Lightfoot et al. [22].

Since the early study of the PAN chemistry it has been shown that the heterogeneous reactivity of peroxyacetyl radical is one of the main difficulties of these studies. Hence, many authors [23–25] had to take into account these phenomena to interpret their results. This fact has led some authors to specifically study the heterogeneous reactivity of the stable and radical species relevant from PAN chemistry [26,27]. Moreover, it has been shown [28] that the heterogeneous reactivity of PA radicals could significantly enhance the gas-phase oxidation of acetaldehyde at higher temperature. Consequently, the chemical system of reactions listed in Table 3 have been completed to take into account these works.

From their experiments in a variable surface-to-volume ratio flow reactor, Langer et al. [26] proposed the mechanism illustrated by Fig. 7.

This hypothesis assumes that PA radicals can find nucleophylic sites to react after adsorption on the wall surface. The break of the weak peroxidic bond would follow this adsorption leaving an oxygen atom adsorbed on the solid surface. Under the Langer's experimental conditions, oxygen atoms are assumed to react with another O^3P to form molecular oxygen. Such a recombination would then regenerate two electron rich sites allowing the process to go on.

In the present work, we have to take account that large quantities of nitric acid are adsorbed on the walls. This assumption is strongly supported by the fact that there is a deficit in the nitrogen balance correlated with the total injected NO_x quantities (see in Fig. 5 the difference between simulated and measured HNO_3). It should be noticed here that 1.5×10^{20} molecules of NO (corresponding to 6.22 cm^3 of gaseous NO) are introduced in the chamber while one HNO_3 monolayer in such a reactor is close to 10^{20} molecules. One must then consider that adsorbed O^{3P}

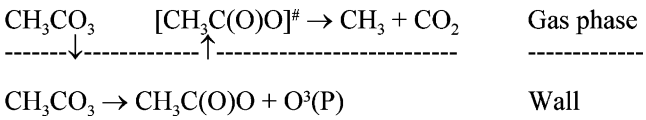

Fig. 7.

could react with adsorbed nitric acid:

$$O^{3P}_{adsorbed} + HNO_{3\,adsorbed} \rightarrow OH_{adsorbed} + NO_{3\,adsorbed} \quad (17)$$

In the gas phase the following lump reactions have been added to the system listed in Table 3:

$$CH_3CO_3(+\,wall + HNO_{3\,adsorbed}) \rightarrow \alpha CH_3C(O)O + \beta OH + \gamma NO_3 \quad (18)$$

The stoechiometric coefficients (α, β and γ) have been adjusted during the fitting process. It should be noticed that β and γ can be different because of the following possible reaction:

$$OH_{adsorbed} + HNO_{3\,adsorbed} \rightarrow H_2O_{adsorbed} + NO_{3\,adsorbed} \quad (19)$$

Such a mechanism allowed us to perform simulations leading to a fairly good agreement with experimental data (see Figs. 4 and 5).

4.2. Kinetic study and comparison with previous work

4.2.1. Uncertainties, sensitivity of the fit and agreement

Fitted values of the rate constants of the studied reactions are given in Tables 4–6 together with the uncertainties. For each experimental results, the error take into account the estimated uncertainties in concentrations determinations, i.e. errors in reactant and product IR absorption band calibration (see Table 1) and in optical path length determination which has been achieved geometrically and verified with N_2O IR absorption. It must be noted that this last uncertainty is negligibly small in comparison with the previous one. The error takes also into account the uncertainties in the numerical simulation estimated by FACSIMILE® by the following procedure: after having calculated the best value of each constant for the fit, the solver makes some further iterations by slightly modifying each fitted constant in order to estimate the sensitivity of the fit to each of them. Using this information, it calculates final uncertainties for a confidence range of 95% (see FACSIMILE v3.0 Technical Reference). During this procedure, the uncertainties on the measurement of the concentrations of the fitted compounds are taken into account by the software.

The overall given errors are determined from the distribution of all the values from each experiment taken with their uncertainties assuming a Gaussian distribution.

The accuracy of the fits has been found to be sensitive to the rate constant reported here. This has been verified through the FACSIMILE® fitting procedure which include a routine to determine whether the data determine the parameter values or not. In short, this procedure varies all the fitted parameter values by a small amount after finding the minimum "sum of square of residuals". From changes in the residuals due to these variations, the software calculate a matrix giving the dependence of the residuals on the parameters values. A test on the singular values of this matrix, excludes the ill-determined parameters from the fit. These matrix calculations are also helpful to determined the linked parameters (see FACSIMILE® v3.0 Technical Reference).

Additionally, the quality of the fit is necessary very sensitive to the rate constant for the reactions between acetaldehyde and NO_3 and between formaldehyde and NO_3 as these three compounds are monitored together. For the reaction between peroxyacetyl radicals and NO_3, the experimental

Table 4
$HCHO + NO_3$: comparison between our results and literature data (all rate constant units are molecule^{-1} cm^3 s^{-1})

(3) $HCHO + NO_3 \rightarrow HNO_3 + HCO$		
$(5.2 \pm 0.9) \times 10^{-16}$	See text	This work
$(3.23 \pm 0.26) \times 10^{-16}$	$(5.0 \pm 0.4) \times 10^{-16}$ Relative rate corrected with new N_2O_5 equilibrium [40]	Atkinson et al. [9]
$(6.3 \pm 1.1) \times 10^{-16}$	Fitted value	Cantrell et al. [7]
$(5.4 \pm 1.1) \times 10^{-16}$	Fitted value	Hjorth et al. [10]

Table 5
$CH_3CHO + NO_3$: comparison between our results and literature data (all rate constant units are molecule^{-1} cm^3 s^{-1})

(4) $CH_3CHO + NO_3 \rightarrow HNO_3 + CH_3CO$		
$(2.1 \pm 0.7) \times 10^{-15}$	See text	This work
$(1.2 \pm 0.3) \times 10^{-15}$	$(2.8 \pm 0.7) \times 10^{-15}$ relative rate corrected with new N_2O_5 equilibrium value [40]	Morris and Niki [13]
$(1.34 \pm 0.28) \times 10^{-15}$	$(2.1 \pm 0.5) \times 10^{-15}$ relative rate corrected with new N_2O_5 equilibrium value [40]	Atkinson et al. [9]
$(2.1 \pm 0.4) \times 10^{-15}$	Fitted value	Cantrell et al. [8]
$(2.74 \pm 0.07) \times 10^{-15}$	Flow reactor (1.2 Torr)	Dlugokenski and Howard [11]
$(2.6 \pm 0.3) \times 10^{-15}$	Relative rate (refer but-1-ene) see Section 4.2.3	D'Anna et al. [12]
$(2.5 \pm 0.5) \times 10^{-15}$	Fast flow discharge	D'Anna et al. [12]
$(3.2 \pm 0.7) \times 10^{-15}$	Fast flow discharge	Cabanas et al. [6]

Table 6
$NO_3 + CH_3C(O)O_2$: comparison between our results and literature data (all rate constant units are molecule^{-1} cm^3 s^{-1})

(6) $NO_3 + CH_3C(O)O_2 \rightarrow CH_3C(O)O + NO_2 + O_2$		
$(3.2 \pm 1.4) \times 10^{-12}$	See text	This work
20×10^{-12}	Slow flow reactor, preliminary study	Biggs et al. [15]
0.15×10^{-12}	Fitted value	D'Anna et al. [12]
$(4 \pm 1) \times 10^{-12}$	Flow reactor	Canosa-Mas et al. [16]

procedure has been adapted to increase the sensitivity of the fit (see Section 3.2).

4.2.2. NO_3-initiated oxidation of formaldehyde

The value of the rate constant of HCHO + NO_3 is in fairly good agreement with previous studies except for the work by Cantrell et al. [7] who obtained results 20% higher. It must be pointed out that the last IUPAC recommendation [29] is $(5.8 \pm 1.7) \times 10^{-16}$ molecule^{-1} cm^3 s^{-1} and seems to be slightly overestimated in comparison with most of the previous results taken together with this work (Table 4).

4.2.3. NO_3-initiated oxidation of acetaldehyde

Our results are in fair agreement with the data reported by Atkinson et al. [9] and Cantrell et al. [8] but seems to be slightly lower than the earlier results by Morris and Niki [13]. The disagreement is more obvious with the low-pressure value from Dlugokenski and Howard [11], which is the only work taken into account by the IUPAC panel to make the recommendation. In spite of the publication of three values [6,12] close to the Duglokenski and Howard [11] rate constant, it is still very difficult to conclude about a recommendation. Indeed, the value published by D'Anna et al. [12] ($(2.6 \pm 0.3) \times 10^{-15}$ molecule^{-1} cm^3 s^{-1}) was calculated with $k_{\text{but-1-ene+NO}_3} = (1.35 \pm 0.10) \times 10^{-14}$ molecule^{-1} cm^3 s^{-1} as reference following the IUPAC recommendation [30] but this last value need to be re-evaluated since some recent absolute determinations [31–33] led to a value around $k_{\text{but-1-ene+NO}_3} = 1.06 \times 10^{-14}$ molecule^{-1} cm^3 s^{-1}. using this value as reference, most of determined values for $k_{\text{CH}_3\text{CHO+NO}_3}$ are around 2.1×10^{-15} molecule^{-1} cm^3 s^{-1} (Table 5).

Furthermore, some of the previous values are relative to the equilibrium constant $K_{2,-2}$ value which is still affected by large uncertainties.

All of the works leading to higher values have been performed at low pressure. Nevertheless, there is no obvious reasons to suspect a pressure effect, even if one takes into account the assumption of an adduct formation made by D'Anna and Nielsen [2] from higher aldehydes results. Further work is needed to clarify this 30% discrepancy between these two groups of values.

4.2.4. Reaction between NO_3 and peroxyacetyl radical

To our knowledge only one group has specifically investigated [16] this reaction. Recently, a twenty time lower estimation of this rate constant has been published [12]. Our work is the first that is performed at atmospheric pressure. Our results are in good agreement with the work of Canosa-Mas et al. [16]. As their experiments were conducted at low pressure and between 404 and 443 K, it is likely that there is neither important pressure effect nor temperature effect on the value of this rate constant. Finally, our study confirms the importance of this reaction under atmospheric conditions (Table 6).

4.2.5. Heterogeneous processes parameters

The apparent rate constants of the hypothetical heterogeneous processes are highly variable from one experience to another. It can be explained by the fact that these phenomena are probably highly dependent from the wall conditioning.

$$0.1\,\text{s}^{-1} < k_{18} < 3\,\text{s}^{-1}$$
$$0.9 < \alpha < 1$$
$$0 < \beta < 0.2$$
$$0.8 < \gamma < 1.1$$

It must be noticed that Langer et al. [26] have proposed the following formula to determine a value for k_{17} in a Pyrex reactor: $k_{17} \leq 7.3 \times$ surface/volume. The S/V ratio for the chamber used in the present work is 0.09 cm^{-1}. According to Langer et al., an upper limit equal to 0.65 s^{-1} is obtained. The fitted k_{18} values ranged from 0.1 to 3 s^{-1} with a median value around 0.6 s^{-1}. One can observe that these results are in the same order of magnitude as those predicted by the Langer's formula. The difference between the predicted and the fitted values can be interpreted as a result of change in the wall conditioning and by the fact that some of the surfaces are not Pyrex but gold (IR mirrors), stainless steel (mechanical parts) or aluminium alloy (UV-visible mirrors, simulation chamber ending flanges).

5. Conclusion

The experiments described here constitute one of the first experimental evidence of the nitrate radical initiated dark production of hydroxyl radicals. It is obvious that the key gas-phase reaction for this phenomenon is the reduction of peroxyacetyl radical by NO_3. Its constant rate has been calculated. The result confirms the importance of this reaction for atmospheric processes, which have been previously shown only one time [16]. Moreover, it should be pointed out that both reactants involved in this reaction (i.e. NO_3 and PA radicals) are in equilibrium with their reservoir species (i.e. N_2O_5 and PAN) through their reaction with NO_2. Furthermore, they are both destroyed by reaction with NO. This indicate that they could be produced under the same conditions (NO/NO_2 ratio, temperature ...), stocked under their reservoir forms in the same air mass and transported away from their sources. Under lower NO_2 level or higher temperature their equilibria lead back to NO_3 and PA radicals and through the process discussed here could induced nighttime OH production at the regional scale.

Acknowledgements

This work has been achieved within the Eurotrac-2 project, sub-project CMD (Chemical Mechanism Development). The authors wish to thank the editors for helpful

comments and Dr. Ian Barnes for sharing information on the N_2O_5 spectroscopy.

References

[1] R.P. Wayne, I. Barnes, P. Biggs, J.P. Burrows, C.E. Canosas-Mas, J. Hjorth, B. Le, G.K. Moortgat, D. Perner, G. Poulet, G. Restelli, H. Sidebottom, Atmos. Environ. 25A (1991) 1–206.
[2] B. D'Anna, C.J. Nielsen, J. Chem. Soc., Faraday Trans. 93 (1997) 3479–3483.
[3] C. Papagni, J. Arey, R. Atkinson, Int. J. Chem. Kinetics 32 (2000) 79–84.
[4] M. Ullerstam, S. Langer, E. Ljungström, Int. J. Chem. Kinetics 35 (2000) 294–303.
[5] B. D'Anna, O. Andresen, Z. Gefen, C.J. Nielsen, Phys. Chem., Chem. Phys. 3 (2001) 3057–3063.
[6] B. Cabanas, P. Martin, S. Salgado, B. Ballesteros, E. Martinez, J. Atmos. Chem. 40 (2001) 23–29.
[7] C.A. Cantrell, W.R. Stockwell, L.G. Anderson, K.L. Busarow, D. Perner, A. Schmeltekopf, J.G. Calvert, H.S. Johnston, J. Phys. Chem. 89 (1985) 139–146.
[8] C.A. Cantrell, J.A. Davidson, K.L. Busarow, J.G. Calvert, J. Geophys. Res. 91 (1986) 5347–5353.
[9] R. Atkinson, C.N. Plum, W.P.L. Carter, A.M. Winer, J.N.J. Pitts, J. Phys. Chem. 88 (1984) 1210–1215.
[10] J. Hjorth, G. Ottobrini, G. Restelli, J. Phys. Chem. 92 (1988) 2669–2672.
[11] E.J. Dlugokenski, C.J. Howard, J. Phys. Chem. 93 (1989) 1091–1096.
[12] B. D'Anna, S. Langer, E. Ljungstroem, C.J. Nielsen, M. Ullerstam, Phys. Chem., Chem. Phys. 3 (2001) 1631–1637.
[13] E.D.J. Morris, H. Niki, J. Phys. Chem. 78 (1974) 1337–1338.
[14] J.S. Gaffney, N.A. Marley, E.W. Prestbo, in: O. Hutzinger (Ed.), The Handbook of Environmental Chemistry, Part B, Air Pollution, vol. 4, Springer, Berlin, 1989, pp. 1–38.
[15] P. Biggs, C.E. Canosa-Mas, K.J. Hansen, P.S. Owen, R.P. Wayne, in: P.M. Borrell, P. Borrell, T. Cvitas, K. Kelly, W. Seiler (Eds.), Eurotrac 94, SPB Academic Publishing, Garmish Partenkirchen, 1994, pp. 139–143.
[16] C.E. Canosa-Mas, M.D. King, R. Lopez, C.J. Percival, R.P. Wayne, D.E. Shallcross, J.A. Pyle, V. Daële, J. Chem. Soc., Faraday Trans. 92 (1996) 2211–2222.
[17] J.F. Doussin, D. Ritz, R. Durand-Jolibois, A. Monod, P. Carlier, Analusis 2 (1997) 236–242.
[18] J.F. Doussin, D. Ritz, P. Carlier, Appl. Opt., Opt. Technol. Div. 38 (1999) 4145–4150.
[19] S.P. Sander, J. Phys. Chem. 090 (1986) 4135–4142.
[20] W.J. Marinelli, D.M. Swanson, H.S. Johnston, J. Chem. Phys. 76 (1982) 2864–2870.
[21] A.R. Curtis, The FACSIMILE Numerical Integrator for Stiff Initial Value Problems, Computer Science and Systems Division, AERE Harwell, 1979.
[22] P.D. Lightfoot, R.A. Cox, J.N. Crowley, M. Destriau, G.D. Hayman, M.E. Jenkin, G.K. Moortgat, F. Zabel, Atmos. Environ. 26A (1992) 1805–1961.
[23] J.J. Orlando, G.S. Tyndall, J.G. Calvert, Atmos. Environ. 26A (1992) 3111–3118.
[24] N. Roumelis, S. Glavas, Monatshefte Fur Chemie 123 (1992) 63–72.
[25] U. Schurath, V. Wipprecht, in: G. Restelli, G. Abgeletti (Eds.), Proceedings of the First European Symposium on Physico-Chemical Behaviour of Atmospheric Pollutants, JRC, Ispra (Italy), 1979, pp. 157–166.
[26] S. Langer, I. Wanberg, E. Ljungstrom, Atmos. Environ. 26A (1992) 3089–3098.
[27] R.H. Bakhchadjyan, I.A. Vardanyan, in: Proceedings of the 14th International Symposium on Gas Kinetics Leeds, UK, 1996.
[28] R.H. Bakhchadjyan, I.A. Vardanyan, Int. J. Chem. Kinetics 26 (1994) 595–603.
[29] R. Atkinson, D.L. Baulch, R.A. Cox, R.F.J. Hanpson, J.A. Kerr, M.J. Rossi, J. Troe, J. Phys. Chem. Reference Data 28 (1999) 191–393.
[30] R. Atkinson, D.L. Baulch, R.A. Cox, R.F.J. Hanpson, J.A. Kerr, M.J. Rossi, J. Troe, J. Phys. Chem. Reference Data 26 (1997) 521–1011.
[31] T. Berndt, I. Kind, H.J. Karbach, Berichte Bunsengeselchaft Physicalische Chemie 102 (1998) 1486–1491.
[32] G. Marston, P.S. Monks, C.E. Canosa-Mas, R.P. Wayne, J. Chem. Soc., Faraday Trans. 89 (1993) 3899–3905.
[33] C.E. Canosa-Mas, P.S. Monks, R.P. Wayne, J. Chem. Soc., Faraday Trans. 88 (1992) 11–14.
[34] I. Barnes Private Communication, 1997.
[35] I. Wängberg, T. Etzkorn, I. Barnes, U. Platt, K.H. Becker, J. Phys. Chem. A 101 (1997) 9694–9698.
[36] J. Hjorth, G. Ottobrini, F. Cappelanni, G. Restelli, J. Phys. Chem. 91 (1987) 1565–1568.
[37] L.S. Rothman, J. Quant. Spectrosc. Radiat. Transf. 48 (1992) 469–507.
[38] B. Picquet-Varrault, J.F. Doussin, R. Durand-Jolibois, O. Pirali, P. Carlier, Environ. Sci. Technol. 36 (2002) 4081–4086.
[39] N. Tsalkani, G. Toupance, Atmos. Environ. 25 (1989) 1849–1854.
[40] S.P. Sander, R. Friedl, W. De More, D.M. Golden, M.J. Kurylo, R.F. Hampson, R.E. Huie, G.K. Moorgat, A.R. Ravishankara, A.R. Kolb, M.J. Molina, Chemical Kinetics and Photochemical Data for Use in Stratospheric Modeling, Jet Propulsion Laboratory, California Institute of Technology, 2000.
[41] R. Atkinson, D.L. Baulch, R.A. Cox, R.F.J. Hanpson, J.A. Kerr, M.J. Rossi, J. Troe, Evaluated Kinetics and Photochemical Data for Atmospheric Chemistry, Supp V—IUPAC Subcommitee on Gas Kinetic Data Evaluation for Atmospheric Chemistry, IUPAC, 2000.
[42] G.K. Moortgat, B. Veyret, R. Lesclaux, Chem. Phys. Lett. 160 (1989) 443–447.